1-1-2003

The influence of bottom morphology on reflectance: Theory and two-dimensional geometry model

J. Ronald V. Zaneveld
Oregon State University

Emmanuel Boss
Oregon State University, emmanuel.boss@maine.edu

Limnol. Oceanogr., 48(1, part 2), 2003, 374–379

The influence of bottom morphology on reflectance: Theory and two-dimensional geometry model

J. Ronald V. Zaneveld and Emmanuel Boss
College of Oceanic and Atmospheric Sciences, Oregon State University, Oceanography Administration Building 104, Corvallis, Oregon 97331-5503

Abstract

The reflectance of the bottom is of importance when interpreting optical data in shallow water. Closure studies of radiative transfer, interpretation of laser line scanner data, lidar, and remote sensing in shallow waters require understanding of the bottom reflectance. In the Coastal Benthic Optical Properties experiment (CoBOP), extensive measurements of the material reflectance (reflectance very close to the bottom) were made. Far field reflectance will be needed in carrying out closure of the radiative transfer model and observed radiometric and inherent optical properties. The far field reflectance is the bottom reflectance that includes the effect of bottom morphology (such as sand ripples) as well as the material reflectance. We present here a first-order analytical model to derive the relationship between the material and far field reflectances. We show that the effective reflectance of the bottom is proportional to the average cosine of the bottom slope. Using a simple two-dimensional geometry without scattering and absorption, we show that errors in ignoring the bottom morphology can lead to overestimations of the far field reflectance on the order of 30%.

Shallow water optical signals are influenced by the bottom reflectivity. Closure of radiative transfer calculations, determination of the contrast of objects with the bottom such as measured by laser line scanners, inversion of remotely sensed radiance for bathymetry, and diver visibility can all be improved with proper knowledge of the bottom reflectance. Many bottoms are nearly Lambertian surfaces, surfaces for which the detected radiance is independent of the viewing angle (Mobley 1994). The radiance reflected from a bottom is not independent of the irradiance impinging on the bottom, however. Therefore, a bottom with topography has a reflectance that is different from a flat, horizontal bottom. Bottom reflectances are usually measured on scales of centimeters (Voss et al. 2000). We call this the material reflectance, although it includes small-scale morphology such as individual grain size. Larger scale morphology, e.g., Wheatcroft (1994), is not included in direct measurements of the bottom reflectance. Radiance and irradiance detectors at larger distances from the bottom will thus see the effect of bottom morphology.

Hapke (1993) has analyzed the reflectance of randomly rough surfaces. He assumed that the distribution function of the facet orientations is independent of azimuth angle and that the two-dimensional azimuth-independent distribution function can be described as a Gaussian distribution multiplied by the sine of the zenith angle of the facets. For vertical illumination and detection, Hapke found that the reflectance relative to a flat bottom was the average cosine of the bottom facets. For different illumination and detection angles, the results are far more complicated. The assumptions made by Hapke do not apply to the regular bottom features we discuss in this paper. Hapke's analysis should be considered, however, in an analysis of the material reflectance of ocean bottoms. Hapke himself questions the validity of his assumption for morphologies with preferred orientations such as fields of parallel sand dunes. Hapke's bottom morphology model needs to be considered for surfaces on millimeter scales, but it does not apply to the nearly coherent longitudinal sand ripples typical of near-shore sandy ocean bottoms. It is the latter case we are interested in analyzing in this paper.

The reflectance of surfaces is a function of both the incident light direction and the emitted light direction. This is the bidirectional reflectance distribution function (BRDF, e.g., Voss et al. 2000). For surfaces where the BRDF is strongly asymmetric, it is obvious that changing the relative incident and emitted light directions, by tilting the bottom, will have a strong effect on the radiance distribution emanating from the bottom. Many bottoms, such as sand, are nearly Lambertian, however (e.g., Mobley 1994). In that case the radiance $L(\theta)$ emanating from the bottom in any direction θ is given by $L(\theta) = \rho E_b/\pi$, where ρ is the material reflectance of the bottom and E_b is the irradiance impinging on the bottom (measured parallel to the bottom). In the simplest case, the incoming light is collimated and vertical and has a downwelling irradiance E_d. The irradiance impinging on the bottom is then $E_b = E_d \cos \theta_b$, where E_b is the irradiance at the bottom and θ_b is the angle of the bottom with the horizontal. Changing the angle of incidence of the incoming light will also change the irradiance and hence the radiance emanating from the bottom. Even in the simplest case it is then seen that the radiance emanating from the bottom depends on all factors that determine the irradiance at the bottom. These factors include the incoming radiance distribution (which in turn is determined by the radiance distribution just above the sea surface, the sea surface, and the inherent optical properties [IOPs] of the water column), the morphology of the bottom, and the geometries of the radiance detector and light source. The theoretical model derived here shows that all these factors are potentially important.

Acknowledgments

This work was supported by the Environmental Optics program of the Office of Naval Research as part of the Coastal Benthic Optical Properties program. We thank W. Philpot and S. Pegau for insightful discussions.

It is the far field reflectance (or effective reflectance) that must be used in radiative transfer calculations when the detector footprint is larger than the bottom roughness scale. For example, in its experimental design, the closure studies of the Coastal Benthic Optical Properties (CoBOP) program did not consider bottom morphology. It is thus worthwhile to evaluate the magnitude of the influence of bottom morphology on plane parallel radiative transfer calculations such as used in CoBOP. Similarly, remote sensing observations that are used to infer bathymetry must also take this into account.

Allen's (1982) monumental review contains ample information on bottom morphology and the associated slopes. The largest bed form slopes are associated with wave ripples and underwater dunes which, on average, have ratios of wavelength to height of about 5. Bottom ripples occur anytime a current moves over a bed of sand, silt, or clay. The specific morphology produced depends on the nature of the bottom and the strength, direction, and duration of the water movement. Wave ripples were the characteristic bed form in the sand flats adjacent to the fringe reefs on the Exuma side of Lee Stocking Island (Bahamas). In contrast, Adderley Cut and Rainbow South were characterized by large shallow underwater dunes. In the former case, a radiance sensor's field of view would cover many ripples, whereas in the latter case, the sensor would likely cover one side of an underwater dune only. Both of these cases will be analyzed in this paper.

Carder et al. (2003) discuss bottom features encountered near Lee Stocking Island (Bahamas) and present results from a Monte Carlo model for the reflectance by a saw-tooth bottom feature. Mobley et al. (2000) showed that for sloping bottoms, the reflectance could be modeled as the reflectance of a horizontal bottom multiplied by the cosine of the slope.

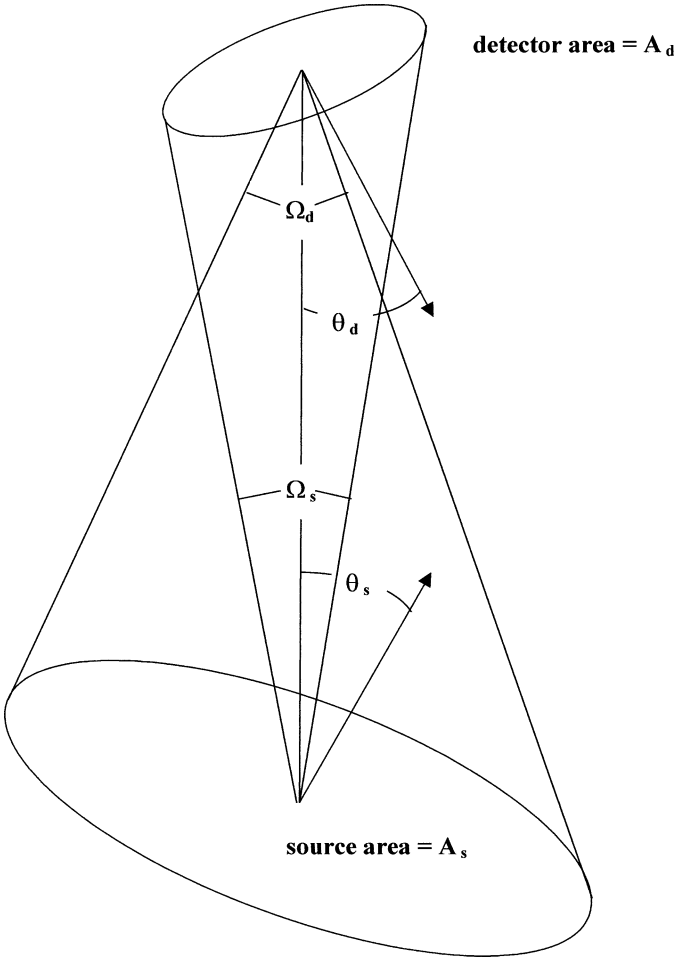

Fig. 1. Geometry for the definition of radiance. For explanation see *Introduction to nomenclature and physics* in the text.

Theory

We will briefly review the definition of radiance in order to set the stage for the subsequent development of the dependence of the far field reflectance on the morphology of the ocean bottom. Figure 1 shows the general geometry of a source and detector system. It is well known (for example, Jerlov 1976) that the radiance is reciprocal, i.e., the radiance from the source to the detector is the same as the radiance from the detector to the source.

We derive here the reflectance observed by a finite radiance detector due to a multifaceted bottom. Secondary reflections of the light by the bottom are ignored. Hapke (1993) has shown that the scattering of light from one facet to another will be small if either the albedo or the mean slope is small. Either or both of these are the case for typical oceanic environments. Light attenuation is also ignored in order to isolate the effect of bottom morphology and hence to derive an effective reflectance that can be used in models in lieu of the usual Lambertian reflectance. Light absorption and scattering can be added in radiative transfer models that can include the sea surface by using the Modulation Transfer Function approach as in Zaneveld et al. (2001).

In the following discussion, the bottom is considered to be the light source as daylight is reflected from it. The radiant flux between a source and a detector is given by Φ. Units are W. The angles θ_d and θ_s are relative to the line connecting the centers of the source and detection areas (Fig. 1). This line need not be perpendicular to the sea surface, as both the detector and the bottom may be tilted relative to the vertical. (*See also* Jerlov 1976 for a good description of the fundamental relationships of radiance.)

Introduction to nomenclature and physics—The source radiance L is defined as the radiant flux per unit solid angle per unit projected area of surface. Units are W m^{-2} sr^{-1}.

The solid angle of the detector is defined as

$$\Omega_d = A_s \cos\,\theta_s / r^2 \tag{1}$$

The projected area of the detector perpendicular to the line joining the centers of the source and the detector is $A_d \cos\,\theta_d$.

The radiance of the source is thus

$$L = \frac{\Phi r^2}{A_d \cos\,\theta_d A_s \cos\,\theta_s} \quad \text{for } A_d \to 0; \qquad A_s \to 0 \tag{2}$$

Note the symmetry in the expression for the radiance. If we interchange the source and detector the expression is the same.

If the source is Lambertian, the radiance in any direction is $L = \rho E_s/\pi$, where ρ is the reflectance of the source (bottom) and E_s is the irradiance at the source (bottom).

We assume that the incoming light is collimated and just below the surface has a solar zenith angle of θ_z. If the collimated irradiance measured perpendicular to the direction of propagation of the photons is E_p, the irradiance at the bottom, E_s, is

$$E_s = E_p \cos|\theta_z - \theta_b| \tag{3}$$

where θ_b is the angle of the bottom with the horizon in the plane of the incoming light. Note that θ_b need not be equal to θ_s, since the line connecting source and detector need not be perpendicular to the sea surface. The absolute value of the difference of the zenith angle and the bottom angle is required since the irradiance is always positive.

Derivation of the general case—The general case requires knowledge of the radiance distribution at the bottom.

The irradiance parallel to the bottom in the general case is given by

$$E_s(x, y, b) = \int_0^{2\pi} \int_0^{\pi/2} L(\theta, \phi, x, y, b) \times \cos|\theta - \theta_b(x, y)| \sin\theta \, d\theta \, d\phi \tag{4}$$

The irradiance at some point (x, y, b) on the bottom thus depends on the local radiance $L(\theta, \phi, x, y, b)$, as well as the local angle of the bottom with the horizon, $\theta_b(x, y)$. For clarity, we will continue our discussion for the collimated radiance case only, although the above expression for E_s for the general case may always be substituted in the equations.

The radiance of the source to the detector in the collimated radiance case is

$$L = \rho E_p \cos|\theta_z - \theta_b|/\pi \tag{5}$$

which by definition is the same as the radiance due to the source perceived at the detector. It is clear that the radiance of the source (bottom) depends on the cosine of the angle of the bottom with the vertical. Note that the radiance does not depend on the solid angle or area of the detector. Equation 5 is the radiance that would be detected in the case of a simple sloping bottom, such as the side of a large underwater sand dune. We then have an effective reflectance equal to

$$\rho_{\text{eff}} = \rho \cos|\theta_z - \theta_b| \tag{6}$$

Hapke (1993) has shown that for vertical illumination and viewing when there are no shadows, and for a two-dimensional azimuth-independent facet distribution function described by a Gaussian distribution multiplied by the sine of the zenith angle of the facet, that the effective cosine of the surface with facets can be described by $\langle \cos\theta \rangle$, where θ is the angle of the normal to a facet with the vertical. For nonvertical illumination and/or viewing the description is far more complicated.

The radiant flux received by the detector as obtained from Eq. 2 and substituting Eq. 5 is

$$\Phi = \frac{L A_d \cos\theta_d A_s \cos\theta_s}{r^2} = \frac{\rho E_p \cos|\theta_z - \theta_b| A_d \cos\theta_d A_s \cos\theta_s}{\pi r^2} \tag{7}$$

A radiance detector measures flux. Commercial detectors are calibrated in terms of radiance, however. For the experimentalist, it is therefore useful to show the result in terms of radiance as well. In practice a radiance detector is not infinitely small. It therefore has a finite detector area and a finite solid angle of detection. This results in the radiance detector averaging the radiance from an area of the bottom, where the bottom may not be flat. What is this average radiance?

A realistic radiance detector's detection solid angle might well simultaneously see several source areas with different slopes. We approximate the bottom as consisting of a number of facets, each with a constant slope angle. Properties such as described in the previous section, but for an individual facet, have the added subscript *i*. The radiant flux from one small source area *i* within the larger detected area to the detector would then be

$$\Phi_i = L_i \Omega_{\text{di}} A_d \cos\theta_{\text{di}} \tag{8}$$

Each individual area would have a radiance L_i and a detection solid angle Ω_{di}, and a normal detection area $A_d \cos\theta_{\text{di}}$. The local radiance would be

$$L_i = \rho E_p \cos|\theta_z - \theta_{\text{bi}}|/\pi \tag{9}$$

Only fluxes from the facets to the detector can be added linearly. Radiance cannot be added linearly, since the solid angles subtended by the facets need not be the same in the general case. The solid angle of detection for the small area *i*, Ω_{di}, is given by

$$\Omega_{\text{di}} = A_{\text{si}} \cos\theta_{\text{si}}/r_i^2 \tag{10}$$

The radiant flux (Watts) received at the detector from the small area *i* is then

$$\Phi_i = \frac{\rho E_p \cos|\theta_z - \theta_{\text{bi}}| A_{\text{si}} \cos\theta_{\text{si}} A_d \cos\theta_{\text{di}}}{\pi r_i^2} \tag{11}$$

Note the parallel between Eqs. 11 and 7. The total flux received by the detector is then

$$\Phi_{\text{total}} = \sum_i \frac{\rho E_p \cos|\theta_z - \theta_{\text{bi}}| A_{\text{si}} \cos\theta_{\text{si}} A_d \cos\theta_{\text{di}}}{\pi r_i^2} \tag{12}$$

The radiance perceived by the finite detector is the total radiant flux divided by the solid angle and detector surface area perpendicular to the line connecting the center of the detector with the center of the total detected area. Substitution of Eq. 12 into Eq. 2 gives

$$L_{\text{meas}} = \sum_{i \in A_s} \frac{\rho r^2 E_p \cos|\theta_z - \theta_{\text{bi}}| A_{\text{si}} \cos\theta_{\text{si}} \cos\theta_{\text{di}}}{\pi r_i^2 \cos\theta_d A_s \cos\theta_s} \tag{13}$$

The detector area canceled, but other simplifications are only possible by assuming simple geometries. The fact that all facets within the bottom area viewed by the radiance detector must be counted is symbolized by $i \in A_s$ in the sum. We remind the reader that parameters with subscripts *i* refer to

individual facets, whereas parameters without that subscript refer to the entire source or detector area parameters. The above expression is only valid for a collimated light field with solar zenith angle θ_z. More complex expressions using the entire light field can be written, but they do not illustrate as well how the various parameters influence the far field reflectance.

We thus conclude that the radiance measured by a finite detector depends on above water lighting conditions and the sea surface through *E,* the bottom morphology through all parameters with subscript *i,* and the detector geometry through all parameters with subscript *d.* When attenuation of the radiance is taken into account, the measured radiance will also depend on the IOP.

Application to real sensors

The definition of radiance (Jerlov 1976; Mobley 1994) implies that both detector and source areas be vanishingly small. Real radiance detectors have finite detector areas and fields of view. The Satlantic model TSRB was widely used during CoBOP for the measurement of downwelling irradiance and upwelling radiance. The radiance detector has a field of view half angle of 5°. The upwelling radiance detector thus sees an area of the bottom that depends on its height above the bottom and may include many small-scale topographic features. Again, we will only consider a collimated incoming radiance field. We conceptually divide the area of the bottom viewed by the radiance detector into a number of equal small areas ΔA_i. These areas are parallel to the surface. Each of these areas ΔA_i is the horizontal projection of a bottom area A_{si}, with a slope θ_{bi}, relative to the horizontal. Radiance detectors should be designed so that their field of view, Ω_d, is small. If that is the case, the individual areas A_{si} within the larger area viewed by the detector have very nearly the same angle θ_{di} between the center of the detector and the center of the small areas. In Eq. 13 we may then set $\cos\,\theta_{di} \approx \cos\,\theta_d$, so that these parameters cancel.

In the case of a TSRB at the surface the distance to the bottom is usually much larger than the height of the bottom morphology features. In that case $r_i \approx r$. If the average bottom is parallel to the sea surface, we may set $\cos\,\theta_s = 1$. Eq. 11 then reduces to

$$L_{\mathrm{TSRB}} = \sum_i \frac{\rho E_p \cos|\theta_z - \theta_{bi}| A_{si} \cos\,\theta_{si}}{\pi A_s} \tag{14}$$

Note that $A_{si}\cos\,\theta_{si} = \Delta A_i$. The small surface areas parallel to the surface add up to the total surface area viewed by the detector

$$A_s = \sum_i A_{si} \cos\,\theta_{si} \tag{15}$$

If we divide the total surface area parallel to the sea surface, A_s, into N equal areas, ΔA, where $\Delta A = A_{si}\cos\,\theta_{si}$, as before, we can further reduce Eq. 14 to

$$L_{\mathrm{TSRB}} = \sum_i \frac{\rho E_p \cos|\theta_z - \theta_{bi}|}{N\pi} = \frac{\rho E_p \langle\cos|\theta_z - \theta_b|\rangle}{\pi} \tag{16}$$

The radiance detected by the TSRB thus does not depend on the angle of the sensor relative to the bottom (or surface), but does depend on the average value of the cosine of the angle of the bottom with respect to the zenith angle of the irradiance, $\langle\cos|\theta_z - \theta_b|\rangle$. We remind the reader that the conclusion is only correct if the irradiance E_p is collimated. In the general case a more complicated expression involving Eq. 4 can be written.

Since the radiance from a Lambertian source is given by $L = \rho E/\pi$, we see that the effective reflectance for a bottom with morphology is

$$\rho_{\mathrm{eff}} = \rho\langle\cos|\theta_z - \theta_b|\rangle \tag{17}$$

It is now also clear that the effect of the IOP did not need to be considered separately for the simple geometry of collimated radiance. We can simply use ρ_{eff} in place of ρ. The effect of the IOP in radiative transfer calculations is precisely the same (provided the morphology is small enough to ignore changed path lengths), only the bottom reflectance has changed. We can thus use standard radiative transfer models, but with the adjusted reflectance.

Analytical two-dimensional geometry model for saw-tooth shaped bottoms

Real bottom morphology requires numerical modeling. By using a simple geometric shape for the bottom, it will be possible to derive analytical expressions for the dependence of the measured reflectance on bottom morphology and viewing angle of the detector. A reasonable approximation is the saw-toothed bottom in which the bottom is piecewise linear with slopes alternately equal to θ_b and $-\theta_b$. For a saw-tooth shaped bottom with amplitude A_b and wavelength L_b, $\theta_b = \mathrm{atan}(4A_b/L_b)$. This bottom has the advantage that all bottom facets have the same absolute slope relative to the horizontal. The far field reflectance (ρ_{ff}) relative to the reflectance of a flat bottom for collimated incident light with a zenith angle of θ_z and for a saw-tooth shaped bottom can be obtained from Eqs. 14, 15, and 16.

$$\rho_{\mathrm{ff}}/\rho = 0.5\,\cos[\theta_z + \mathrm{atan}(4A_b/L_b)] + 0.5\,\cos[\theta_z - \mathrm{atan}(4A_b/L_b)] \tag{18}$$

A similar expression for a sinusoidal bottom with amplitude A_b and wavelength L_b is

$$\frac{\rho_{\mathrm{ff}}}{\rho} = \left(\frac{1}{2\pi}\right)\int_0^{2\pi} \cos\left\{\theta_z + \mathrm{atan}\left[\left(\frac{2\pi A_b}{L_b}\right)\sin\left(\frac{2\pi x}{L_b}\right)\right]\right\} dx \tag{19}$$

For a saw-tooth wave and zenith sun, we can thus readily calculate the effective reflectance. The average cosine of the bottom slope is simply the cosine of the saw tooth with the horizontal. An approximate angle of repose for sand is 34°, but can be much higher if the organic content is high (R. Wheatcroft pers. comm.). Use of such a value is also supported by Allen (1982). We can thus approximate the ratio of the far field reflectances of a saw-tooth shaped bottom at a 34° angle and a flat bottom as being $\cos 34 = 0.829$. Thus the reflectance of the saw-toothed bottom is about 17% smaller than that of a flat bottom. The decrease in reflectance

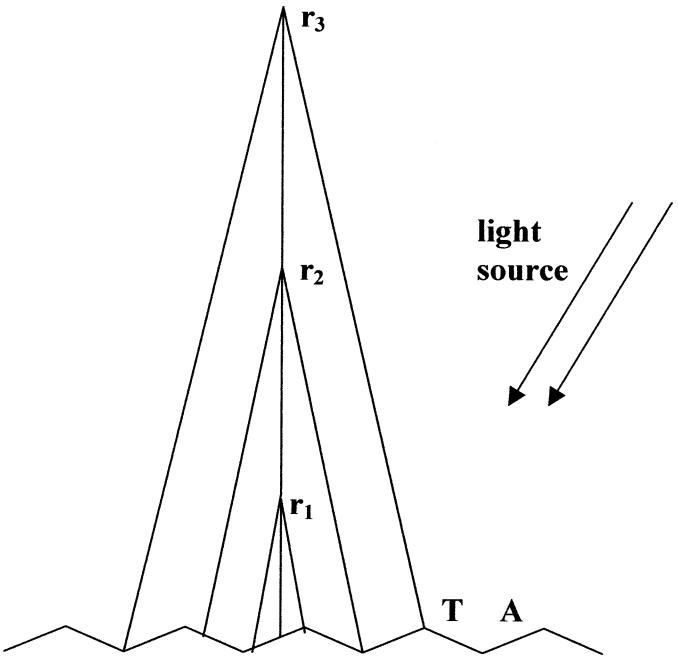

Fig. 2. When a downward looking detector is alternately placed at r1, r2, and r3, successively more bottom facets are in its field of view. These facets either point toward (*T*) or away (*A*) from the source. The effective reflectance depends on the detector distance from the bottom, the placement of the perpendicular from the sensor to the average bottom relative to the crest of the saw tooth, the slope of the saw-tooth facets with the horizontal, and the material reflectance of the bottom.

is 23% if the bottom angle increases to 40°. If the zenith angle of the irradiance striking the bottom is 20°, Eq. 18 shows that the ratio of the reflectances would be about 22% for a 34° bottom slope and 28% for a 40° bottom slope. These values give a rough indication of the range of errors to be expected when bottom morphology is ignored. Numerical results for sinusoidal bottoms with the same amplitudes and wavelengths as a saw tooth are within a few percent. Equation 18 is thus useful for estimating potential errors in a given location, if the bottom morphology is known. Note that the presence of morphology always results in lower far field reflectances and hence a ''darker'' looking bottom. Far field implies that the sensor sees a large number of facets. In the next section we will consider the resultant reflection when the sensor views only a limited number of bottom facets.

Near field reflectance—Let us again consider the saw-tooth bottom as a simple example that lends itself readily to analysis. If the IOPs are ignored, distance from the bottom can be used to estimate the effect of including more bottom features in the field of view of the sensor. Figure 2 shows the near field radiance detector situation. As the detector distance from the bottom increases, its footprint will include more and more facets. These facets are either turned toward the light source or away from the source. The number of bottom facets included in the reflectance influences the effective reflectance. Consider incoming light irradiating the bottom from one side. Equation 16 shows that very near the bottom one would either be looking at a facet toward the incoming irradiance or away from it. The reflectance thus would be $\cos[\theta_z + \text{atan}(4A_b/L_b)]$ or $\cos[\theta_z - \text{atan}(4A_b/L_b)]$.

As one backed away from the bottom, more and more facets would come into view, with the reflectance eventually reaching the far field value of Eq. 18. The reflectance as a function of distance from the bottom would thus be an oscillatory function. A saw-tooth bottom in the plane of the irradiance has facets toward the sun and facets away from the sun. If the linear dimension of the footprint of the sensor on the bottom is given by P when the sensor is a distance r above the bottom, and the wavelength of the saw-tooth bottom is L_b, the sensors would view $2P/L_b$ facets. If the number of facets in view toward the sun is given by N_T and those away from the sun by N_A, then $N_T + N_A = 2P/L_b$. The bottom reflectance will then be

$$\rho_{\text{eff}}(r)/\rho = (L_b N_T/2P)\cos[\theta_z + \text{atan}(4A_b/L_b)] + (L_b N_A/2P)\cos[\theta_z - \text{atan}(4A_b/L_b)] \quad (20)$$

At most, for any given distance from the bottom, the sensor can see one more facet of one kind than the other, hence the maximum reflectance is measured when $N_T = N_A + 1$, and the minimum when $N_A = N_T + 1$. At a distance r from the bottom, the maximum reflectance that could be observed would then be

$$[\rho_{\text{eff}}(r)/\rho]_{\max} = \rho_{\text{ff}}/\rho + (L_b/4P)\cos[\theta_z + \text{atan}(4A_b/L_b)] - (L_b/4P)\cos[\theta_z - \text{atan}(4A_b/L_b)] \quad (21)$$

The minimum reflectance that could be observed would be

$$[\rho_{\text{eff}}(r)/\rho]_{\min} = \rho_{\text{ff}}/\rho - (L_b/4P)\cos[\theta_z + \text{atan}(4A_b/L_b)] + (L_b/4P)\cos[\theta_z - \text{atan}(4A_b/L_b)] \quad (22)$$

The maximum and minimum errors thus change proportionately to $L/4P$. If the half angle of the detector is given by γ, $P = 2r \tan \gamma$, so that the maximum error is proportional to L_b/r and hence the measured reflectances approach the far field reflectance for large r. Figure 3 shows this effect for a typical calculation. The figure furthermore shows that the error depends also on the placement of the sensor relative to the crests and troughs of the bottom. If initially the sensor is placed at the top of the crest, and is backed away, the observed reflectance would always be the far field reflectance, because an equal proportion of facets toward and away from the irradiance would always be seen. If, however, the sensor is initially placed facing the center of a facet, as it is backed away from the bottom, the maximum and minimum reflectances as shown in Eqs. 21 and 22 will be encountered alternatively. Placements in between these extremes results in a truncated saw tooth for the effective reflectance as the detector is backed away from the bottom (Fig. 3). This phase error is proportional to the distance of the vertical projection of the center of the sensor and the center of a facet. This shows that in the near field, placement of the sensor relative to the bottom morphology has a major influence on the measured reflectance.

Discussion

In this paper we have ignored the effects of absorption and scattering. The reflectance or BRDF of a bottom does not

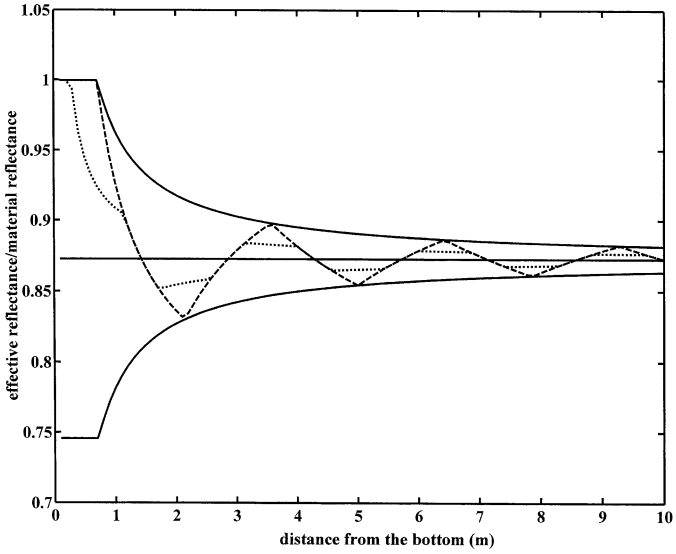

Fig. 3. Example of near field effective reflection relative to the material reflection as a function of distance from the bottom for a saw-tooth bottom with an amplitude of 0.025 m and a wavelength of 0.25 m. The detector has a 5° half angle field of view. The upper and lower curves are the maximum and minimum reflectances that can be detected. The far field reflectance relative to the near material reflectance is 0.75. This is always the relative reflectance if the detector is located directly above the interface of two facets. Maximum variability is obtained when the detector is located directly above the center of a facet (dashed line). The relative reflectance is truncated when the detector is neither directly above the edge or center of a facet. The dotted line is for a detector that is directly above a point 0.2 wavelengths from the edge of a facet.

involve the IOP of the water column. It thus was of interest to derive an equivalent expression for the far field reflectance of a bottom with morphology. This was possible only for parallel radiance. Light scattering redirects radiance. Equation 4 shows that light scattering, which is symmetric about the original direction, will result in decreased radiance reflected from the bottom. On the other hand, light absorption tends to decrease the zenith angle of the radiance. This can increase or decrease the reflected radiance depending on $|\theta_z - \theta_b|$.

We have shown that the effect of bottom morphology on the far field or effective reflectance can be substantial and cannot be ignored. We examined simple cases in which the radiance field was collimated and could be described by a single parameter, the zenith angle θ_z. Similarly we examined a simple bottom form, the saw tooth, whose slope could be described by the single angle θ_b. Depending on wavelength and amplitude, this can be an approximation for both sand ripples and much larger underwater sand dunes. This resulted in the simple expression Eq. 17 for the far field reflectance. We showed that for a flat sea surface and a saw-tooth bottom with a slope around the angle of repose for loose sand, the far field reflectance can be approximately 20% smaller than the material reflectance. If there are organic materials in the bottom sediment, the angle of repose can be much larger (R. Wheatcroft pers. comm.) and the far field reflectance can decrease much more. We showed that if the angle of incidence of the radiance changes away from the vertical, the far field reflectance is reduced further. In general we can thus conclude that the larger the average cosine of the light field and the larger the average slope of the bottom, the larger the deviation of the far field reflectance from the material reflectance. This would thus be a guide for where to carry out closure experiments without the influence of bottom morphology.

In the near field, the reflectance depends on the horizontal and vertical placement of the sensor. This leads to the important conclusion that at least in the near field, the bottom morphology cannot be dealt with in a statistical manner. It is important whether or not the field of view of the radiance sensor primarily sees facets toward the illumination or away from it. This effect is obviously more important the larger the wavelengths of the bottom features.

In the general case, the radiance is not collimated and the bottom is not simply described. The general case solution for a Lambertian bottom is obtained by substituting $E_p\cos|\theta_z - \theta_b|$ in Eq. 13 by $E_s(x, y, b)$ as obtained from Eq. 4. The general case is clearly much more complicated and can only be solved by means of numerical calculations. In addition, if the bottom is not Lambertian one must use the BRDF.

When dealing with shallow waters one has the additional complication of surface waves. In shallow waters with waves, the light field is clearly not homogeneous horizontally, and the plane parallel assumption does not hold (Zaneveld et al. 2001). This manifests itself through the light and dark patterns seen on the bottom in shallow waters (the swimming pool bottom effect). There is a nonlinear interaction between these patterns and the bottom. Equation 4 shows that one could average over time and obtain a long-term average far field reflectance. The nonlinearity of the problem shows that one cannot simply separate the average characteristics of the light field and the average characteristics of the bottom. Analysis of the general case by means of numerical models will be the subject of future study.

References

ALLEN, J. R. L. 1982. Sedimentary structures, v. 1. Elsevier.

CARDER, K. L., AND OTHERS. 2003. Illumination and turbidity effects on observing faceted bottom elements with uniform Lambertian albedos. Limnol. Oceanogr. **48:** 355–363.

HAPKE, B. 1993. Theory of reflectance and emittance spectroscopy. Cambridge Univ. Press.

JERLOV, N. G. 1976. Marine optics. Elsevier.

MOBLEY, C. D. 1994. Light and water. Academic.

———, L. SUNDMAN, H. ZHANG, AND K. J. VOSS. 2000. Effects of optically shallow bottoms on water-leaving radiances. Ocean Optics XV.

VOSS, K. J., AND OTHERS. 2000. Instrument to measure the bidirectional reflectance distribution function. Appl. Opt. **39:** 6197–6206.

WHEATCROFT, R. A. 1994. Temporal variation in bed form configuration and one-dimensional bottom roughness at the mid-shelf STRESS site. Cont. Shelf Res. **14:** 1167–1190.

ZANEVELD, J. R. V., E. BOSS, AND A. BARNARD. 2001. Influence of surface waves on measured and modeled irradiance profiles. Appl. Opt. **40:** 1442–1449.

Received: 4 August 2001
Accepted: 3 April 2002
Amended: 25 April 2002